# The water oxidation kinetics of accumulated holes on the surface of a $TiO_2$ photoanode: A rate law analysis

*Andreas Kafizas,[a]* Yimeng Ma,[a] Ernest Pastor,[a] Stephanie R. Pendlebury,[a] Camilo Mesa,[a] Laia Francàs,[a] Florian Le Formal,[b] Nuruzzaman Noor,[c] Min Ling,[c] Carlos Sotelo-Vazquez,[c] Claire J. Carmalt,[c] Ivan P. Parkin[c] and James R. Durrant[a]**

[a]Department of Chemistry, Imperial College London, South Kensington Campus, London, SW7 2AZ, UK

[b]Laboratory for Molecular Engineering of Optoelectronic Nanomaterials, Ecole Polytechnique Fédérale de Lausanne, Lausanne, Switzerland

[c]Department of Chemistry, University College London, 20 Gordon Street, London, WC1H 0AJ, UK

*corresponding authors: a.kafizas@imperial.ac.uk, j.durrant@imperial.ac.uk

ABSTRACT. It has been more than 40 years since Fujishima and Honda demonstrated water splitting using $TiO_2$, yet there is still no clear mechanism by which surface holes on $TiO_2$ oxidize water. In this article, we use a range of complementary techniques to study this reaction that provide a unique insight into the reaction mechanism. Using transient photocurrent (TPC) and

transient absorption spectroscopy (TAS), we measure both the kinetics of electron extraction ($t_{50\%}$ ~200 µs, 1.5 $V_{RHE}$) and the kinetics of hole oxidation of water ($t_{50\%}$ ~100 ms, 1.5 $V_{RHE}$) as a function of applied potential, demonstrating the water oxidation by $TiO_2$ holes is the kinetic bottleneck in this water splitting system. Photo-induced absorption spectroscopy (PIAS) measurements under 5 s LED irradiation are used to monitor the accumulation of surface $TiO_2$ holes under conditions of photo-electrochemical water oxidation. Under these conditions we find that the surface density of these holes increases non-linearly with photocurrent density. In alkali (pH 13.6), this corresponded to a rate law for water oxidation that is 3rd order with respect to surface hole density, with a rate constant $k_{WO}$ = 22 ± 2 $nm^4.s^{-1}$. Under neutral (pH = 6.7) and acidic (pH = 0.6) conditions the rate law was 2nd order with respect to surface hole density, indicative of a change in reaction mechanism. Although a change in reaction order was observed, the rate of reaction did not change significantly over the wide pH range examined (with TOFs per surface hole in the region of 20 – 25 $s^{-1}$ at ~1 sun irradiance). This showed that the rate limiting step does not involve $OH^-$ nucleophilic attack and demonstrated the versatility of $TiO_2$ as an active water oxidation photocatalyst over a wide range of pH.

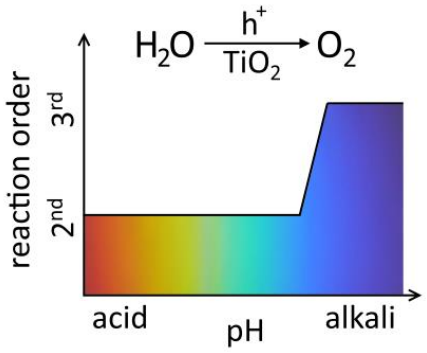


TOC graphic

KEYWORDS: $TiO_2$, water oxidation kinetics, rate law, charge carrier dynamics, photoanode

## 1. INTRODUCTION

The photo-induced oxidation of water on $TiO_2$ has attracted a great deal of interest since Fujishima and Honda's pioneering work more than 40 years ago.[1] It is a versatile material, showing activity for a range of photocatalytic applications (*e.g.* water remediation, air purification devices, and self-cleaning/ antimicrobial surfaces), and is non-toxic, cheap, robust and stable over a wide range of pH and voltage.[2] One drawback is the wide bandgap ($\geq$ 3.0 eV), which severely limits the amount of sunlight it can utilize ($\leq$ 5% of photons).[3] To achieve commercially relevant solar-to-hydrogen efficiencies in a water splitting tandem cell, the ideal bandgaps of the two light absorbing materials should be 1.7 and 1.0 eV respectively.[4] In an effort to decrease the bandgap of $TiO_2$, and increase solar activity, $TiO_2$ has been doped with nitrogen,[5,6] sulphur,[7] fluorine[8] and other elements.[9,10] However, coupling $TiO_2$ with narrow bandgap semiconductors and forming heterojunctions can result in synergistic improvements in activity, and may be the more promising strategy.[11,12]

Since the first definitive proof that photocatalytic water oxidation in plants occurs on a manganese cluster (photo-system II),[13] numerous mimics have emerged.[14,15] Interest in solar driven fuel synthesis has stimulated the investigation of photocatalysts capable of oxidizing water under solar irradiation, including, in particular, metal oxides due to their stability under oxidizing conditions.[16,17] However, recent research has shown that many metal oxide photocatalysts possess slow reaction kinetics when oxidizing water (typically > 100 ms).[18] The use of surface co-catalysts, such as Ni:FeOOH[19] and cobalt phosphate,[20] can improve the activity of photoanode materials. Recent studies have shown that ion-permeable co-catalysts, such as nickel hydroxide, can form adaptive junctions where the barrier to charge transfer changes with

the oxidation state of the co-catalyst.[21] Therefore, the design and synthesis of more efficient solar water splitting systems requires a deeper understanding of the water oxidation process; often considered a "*kinetic bottleneck*" in the overall water splitting reaction.[22] There have been several studies of the water oxidation reaction mechanism on $TiO_2$, using electrochemical[23–25] and spectroscopic[26–35] methods, yet a detailed understanding of the reaction mechanism remains elusive.

While rate law analyses of water oxidation are rare,[36,37] there is growing evidence that lower energy pathways to photocatalytic water oxidation requires the accumulation of multiple holes or oxidizing equivalents.[22] In this study, we present the first rate law analysis of photocatalytic water oxidation on anatase $TiO_2$ using photo-induced absorption spectroscopy (PIAS). The method relies on simultaneously monitoring the absorption of photo-generated holes and the photocurrent density under quasi-steady conditions of photo-electrochemical water oxidation. This novel approach was recently used to examine the reaction kinetics, and thus deduce the rate law with respect to holes, for the photocatalytic oxidation of water on $\alpha$-$Fe_2O_3$ in alkali[36] and on $BiVO_4$ in neutral pH.[37]

Using PIAS, we investigate the water oxidation reaction on anatase $TiO_2$ in acid, neutral and alkali pH. To our knowledge, this is the first rate law analysis of the water oxidation reaction with respect to holes at varied pH. In acidic and neutral conditions, a second order reaction was observed with respect to holes. In alkaline conditions, a third order reaction was observed. Overall, we conclude that the oxidation of water on $TiO_2$ requires multiple holes (or oxidized equivalents) to accumulate and overcome the rate-limiting step; consistent with recent observations of peroxo and oxyhydroxo intermediates on $TiO_2$ and other metal oxide surfaces during water oxidation using *in situ* transient FT-IR spectroscopy.[38,39] Although the reaction

order changes with pH, the rates of reaction were similar over the range of light intensities examined (~0.001 – 1 sun). This showed that hydroxyl nucleophilic attack is most probably not included in the RLS, demonstrating the versatility of $TiO_2$ as an equally active water oxidation photocatalyst over a wide range of pH.

## 2. EXPERIMENTAL

Information on the synthesis and physical characterization techniques are provided in the supplementary information. All functional analyses were carried out in a home-made PEEK cell with quartz windows. Three aqueous electrolytes were examined; 1 M NaOH for studies in alkali (pH = 13.6), 0.05 M $K_2HPO_4$ & 0.05 M $KH_2PO_4$ for studies in neutral (pH = 6.7) and 0.5 M $H_2SO_4$ for studies in acid (pH = 0.6). A three-electrode configuration was used, with a Pt mesh counter electrode, a Ag/AgCl/saturated-KCl reference electrode (0.197 $V_{NHE}$ at 25 °C; Metrohm) and the anatase $TiO_2$ photoanode as the working electrode. Full details of our functional characterization methods (including our photoelectrochemical, electrochemical impedance, transient photocurrent, transient absorption spectroscopy and photo-induced absorption spectroscopy studies) are provided in the supporting information.

## 3. RESULTS AND DISCUSSION

### 3.1. Physical characterization

A dense and flat $TiO_2$ photoanode, of the anatase crystal phase, was grown on an FTO electrode by atmospheric pressure chemical vapor deposition. Before studying the catalytic activity, it was important that we characterized the material in as much detail as possible.

The crystal structure was confirmed by XRD and Raman spectroscopy (Figure S1); with almost no impurity elements observed by XPS (< 1% carbon in bulk). AFM showed that the surface was highly smooth (Figure S2). The surface was further investigated by HRTEM (Figure 1). Primarily the (101) crystal plane was observed, where the measured lattice spacing of 3.48 Å was consistent with literature standards (Figure S3).[40] A thin layer of amorphous material (~1 nm thick) was observed on the material surface, which was attributed to either surface defects or adventitious impurities. From UV-visible absorption measurements, the bandgap was derived using a Tauc plot[41] and was similar to literature reports (~3.2 eV, Figure S4).[2] From the oscillations observed in UV-visible absorption spectroscopy, film thickness was determined using the Swanepoel method (~1 μm, Figure S5).[42] The flat-band potential and donor density were determined from Mott-Schottky analysis to be $V_{fb}$ ~0.4 $V_{RHE}$ and $N_D$ ~2 x $10^{19}$ $cm^{-3}$ respectively, similar to previous reports (Figure S6).[43] A summary of these physical properties are shown in Table S1.

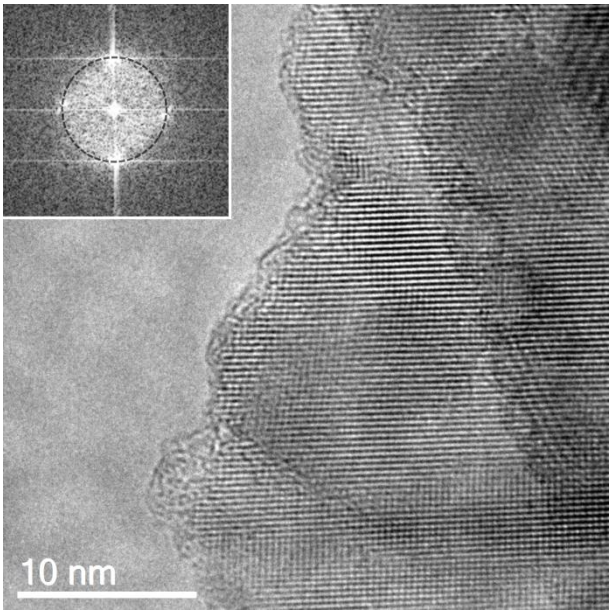


**Figure 1**. HRTEM image of the surface of the $TiO_2$ photoanode and the corresponding Fourier transformation (inset) revealing the preferred growth in the anatase (101) crystal plane.

### 3.2. Functional characterization – the water oxidation reaction

*3.2.1. Photoelectrochemistry*

We first investigated the photoelectrochemical response of our $TiO_2$ photoanode in its oxidation of water (Figure 2). The onset potential of photocatalytic water oxidation was observed from 0.2 $V_{RHE}$, and the photocurrent plateaued from roughly 0.8 $V_{RHE}$ and above. When fixing the applied potential at 1.5 $V_{RHE}$, the APCE approached unity from ≤ 310 nm (Figure S7). However, it should be noted that at 355 and 365 nm (the respective wavelengths of the laser and LEDs used in our studies of the water oxidation mechanism) the respective APCEs were 16 and 7%.

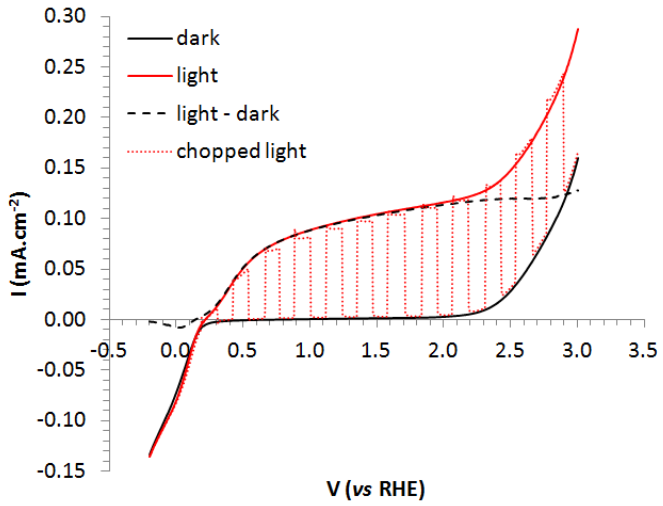


**Figure 2**. The photo-electrochemical response of the anatase $TiO_2$ photoanode vs applied potential ($V_{RHE}$) using a continuous wave 365 nm LED light source (8.0 $mW.cm^{-2}$) in 1 M NaOH (pH = 13.6). Measurements were performed in the dark (black line), light (red line) and chopped-light (red dashed-line) conditions. The photocurrent of light minus dark measurements is also shown (black dashed-line).

*3.2.2. Transient photocurrent and transient absorption spectroscopy*

In order to understand the catalytic activity of surface holes, and their reaction with water, we first need to identify the conditions and timescales in which holes accumulate at the surface of the material and react. As such, the dynamics of both electron and hole carriers were first studied using transient photocurrent (TPC) and transient absorption spectroscopy (TAS).

The TPC was measured following ultra-bandgap laser pulse excitation (355 nm, 3.49 eV). This allowed us to measure both the kinetics and magnitude of electron extraction at various applied potentials (0.10 – 1.5 $V_{RHE}$, Figure S8). Integration of these transient photocurrents allows us to plot the kinetics and relative yields of electron extraction (Figure 3a). As the applied potential was increased from 0.30 to 1.5 $V_{RHE}$, the kinetics of electron extraction marginally increased (with half-times decreasing from $t_{50\%}$ ~400 μs to ~200 μs), however, the amount of electrons extracted increased substantially (from ~3.0 to ~9.6 $\mu C.cm^{-2}$). For a given applied potential, the amount of electron extraction increased linearly with light intensity (Figure S9). At low applied potentials, below 0.8 $V_{RHE}$, our TPC studies showed a reverse (negative) flow at early times corresponding to back-electron flow from the external circuit into the $TiO_2$ photoanode (Figure 3a), also apparent as a modest drop in electron extraction yield observed on the millisecond to second timescale for these potentials in Figure 3a. This phenomenon of back-electron flow was further investigated by chopping a continuous wave LED light (Figure S10). The back-electron flow into the photoanode was suppressed at applied biases ≥ 0.8 $V_{RHE}$. This phenomenon has previously been observed in α-$Fe_2O_3$ and $BiVO_4$ photoanodes,[44–46] and is caused by the recombination of electrons in the photoanode bulk with surface accumulated holes (sometimes called surface or back electron hole recombination). Overall the increase in electron extraction efficiency with increasingly positive applied bias in the $TiO_2$ photoanodes studied herein is

assigned not to faster electron extraction but rather slower recombination kinetics, resulting in both more efficient hole transfer to the surface and longer lifetimes for those holes which reach the surface.

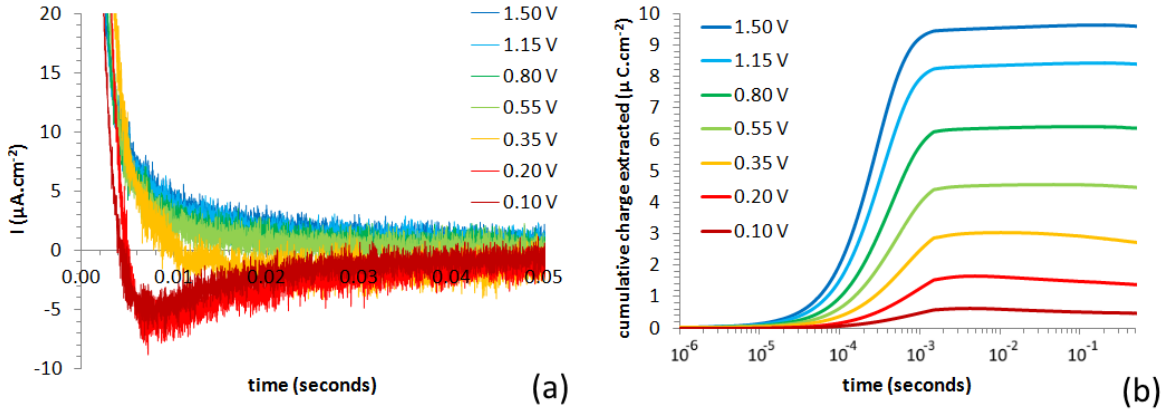


**Figure 3**. (a) The transient photocurrent measured for the anatase $TiO_2$ photoanode in 1 M NaOH (pH = 13.6) at various applied potentials ($V_{RHE}$) using a laser excitation pulse (355 nm, 6 ns pulse width, 1.98 $mJ.cm^{-2}$). (b) The cumulative charge extracted, determined by integrating the transient photocurrent.

Using TAS, the dynamics of photo-generated charge carriers in $TiO_2$ can be studied by tracking transient changes in optical absorbance following pulsed laser excitation.[47] The regions in which photo-generated electrons and holes absorb can be resolved using chemical scavengers (*e.g.* methanol – a hole scavenger; silver nitrate – an electron scavenger), where previous transient absorption studies have shown that electrons and holes show broad absorptions centred at ~800 and ~500 nm respectively.[48] Previous *in situ* TAS studies of the water oxidation reaction on $TiO_2$ show that the absorption of holes at ~500 nm increases with applied potential, where the population of long-lived holes tracked the current-voltage curve.[49] In the study herein, we focus on the long-lived (millisecond to second) charge carriers responsible for photocatalytic water oxidation on $TiO_2$,[50,51] akin to several other metal oxide surfaces such as $BiVO_4$[45] and $\alpha$-$Fe_2O_3$.[52]

The transient absorption kinetics of our anatase $TiO_2$ photoanode was examined at various applied potentials (Figure 4), plotted as function of probe wavelength at a time delay of 100 ms in Figure 4a, and as a function of time for one probe wavelength (500 nm, corresponding to $TiO_2$ hole absorption) in Figure 4b . The transient decays at 0.3 $V_{RHE}$ (Figure 4a) were analogous to those found at open-circuit (Figure S11). This showed that the transient absorption kinetics below the flat-band potential (< 0.4 $V_{RHE}$) related mostly to back electron hole recombination, which was in agrement with our PEC studies (Figure 2). At potentials more negative than flat-band, back electron hole recombination was more rapid, as band-bending was absent (Figure 4a). At more positive potentials (≥ 0.70 $V_{RHE}$), recombination was inhibited due to increased band-bending and stronger electric fields in this space charge layer, significantly increasing the yield and lifetimes of photo-generated holes observed on these timescales (Figure 4b); an effect similary observed in previous studies of mesoporous anatase $TiO_2$ photoanodes.[53] The increase in yield can be attributed to an improved efficiency of hole transfer to the surface, and the increase in lifetime to the inhibition of back electron hole recombination, consistent with the photocurrent data in Figure 3 above.

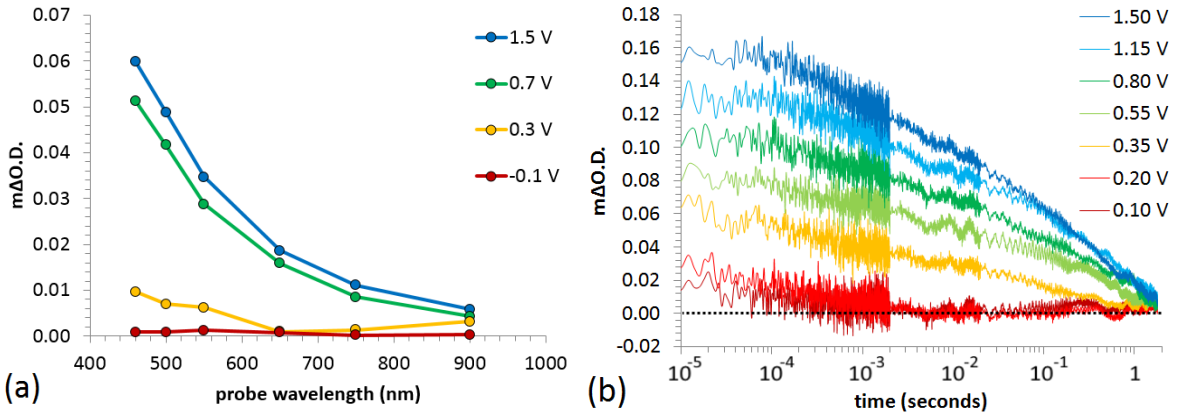


**Figure 4**. Transient absorption spectroscopy data for anatase $TiO_2$ photoanodes measured in 1 M NaOH (pH = 13.6) at various applied potentials ($V_{RHE}$) using a laser excitation pulse (355 nm, 6

ns pulse width, 1.98 mJ.cm$^{-2}$). (a) Spectra observed 100 ms after the laser pulse. (b) Decay kinetics of holes measured at a probe wavelength of 500 nm.

Above the onset potential for water oxidation (> 0.3 $V_{RHE}$), the lifetime of photo-generated holes increases substantially with applied potential ($t_{50\%}$ = 0.5 ms at 0.35 $V_{RHE}$, whereas $t_{50\%}$ = 85 ms at 1.5 $V_{RHE}$ determined as the decay half-time on the measured timescale from 10 μs – 1 s), see Figure 4b. Transient absorption decays were measured at 1.5 $_{RHE}$ for different probe wavelengths (Figure S12); Different transient absorption decay kinetics are observed at different wavelengths. This is attributed to the differing behaviour of photo-generated electrons and holes. The electron signal at ~800 nm mostly decays within 1 ms. However, the hole signal at ~500 nm is much longer lived, decaying most rapidly from 100 ms. Of note, this behaviour was disparingly different from what was observed at open-circuit, where the decay kinetics were equivalent at all wavelengths, as solely electron-hole recombination can occur (Figure S11). However, at 1.5 $V_{RHE}$, there is substantially less electron-hole recombination, which is reflected in the long-lived hole signal observed at ~500 nm (Figure S12). Our TPC studies showed that photo-generated electrons are mostly extracted within 1 ms (Figure 3b), which correlates with our TAS studies that show our electron signal had mostly decayed by 1 ms. From 1 ms onwards, a strong signal due to photo-generated holes was still observed at 500 nm. As the electron signal had mostly decayed by 1 ms, and back electron hole recombination was turned off at strong anodic bias, the loss of the hole signal from the ms – s timescale was attributed to the reaction of holes with water. The yield of these long lived holes, as monitored by their transient absorption at 500 nm, tracked the space charge layer width (Figure S13), indicating that these long lived holes result from photons absorbed within or near the space charge layer. This is in agreement with previous fs-TAS studies which showed that, in the absence of space charge layer formation,

more than 50% of photo-generated $TiO_2$ charges recombine before 1 ns at similar laser powers.[54] The long lifetime of the surface holes studied herein differs from a previous study of mesoporous anatase photoanodes, where from ~10 μs more than 80% of the hole signal was lost due to back electron hole recombination under similarly anodic bias.[53] We attribute this difference to the enhanced spatial separation of charge afforded by the dense flat photoanode structure employed herein, which allows efficient charge separation by the electrical field within the space charge layer.

The kinetics of photocatalytic water oxidation by holes was at least two orders of magnitude slower than electron extraction, with a $t_{50\%}$ of ~100 ms similar to previous studies.[53] This shows that the oxidation of water by holes is the bottle-neck for the overall reaction in anatase $TiO_2$. These kinetics followed a stretch-exponential decay model (Figure S14, Table S2). Comparing the magnitude of electron extraction (Figure S9) with our photo-generated hole signals (Figure S14) we could estimate the extinction coefficient of holes in anatase $TiO_2$ ($\varepsilon_{h+}$ ~2000 $M^{-1}.cm^{-1}$, Figure S15).

*3.2.3. Photo-induced absorption spectroscopy*

Photo-induced absorption spectroscopy (PIAS) was used to determine the reaction order and kinetics (with respect to surface accumulated holes) of the water oxidation reaction on $TiO_2$.

The optical absorption of photo-generated charge was investigated using continuous wave illumination (as opposed to pulsed-laser excitation used in our TAS and TPC studies). This was in order to study the behavior of charge carriers at conditions typical to an applied device (*i.e.* continuous wave solar light). Instead of the short laser pulse used in our TPC and TAS studies (6 ns pulse width), a continuous wave source was turned on and off for periods of several seconds; a period of time sufficient to reach the steady state of catalysis. The photo-induced

absorption spectra (PIAS) measured after ~5 s of illumination and at several applied potentials (Figure S16) were similar to those measured by TAS (Figure S11b), and showed that the states observed at 500 nm were also photo-generated holes. The PIA behavior of these holes, when the $TiO_2$ photoanode is held at 1.5 $V_{RHE}$ in alkali (1 M NaOH, pH = 13.6), is shown in Figure 5a for several light intensities. When the light is turned on (at 0 s), the hole density increases until it plateaus at a steady-state (2 – 6 s). When the light is turned off, the hole density decreases, assigned to their dissipative reaction with water (6 – 10 s). During our PIAS measurements, the photocurrent was measured simultaneously. Changes in photocurrent were sharper than changes in hole density, reaching a steady-state almost instantaneously as the light source was turned on and off (Figure 5b). The region where the hole signal reaches a plateau (~1 s after the light is turned on) is deemed the steady state, as the flux of electrons and holes reaches an equilibrium. At the highest light intensities, this plateau region corresponds to a steady-state hole concentration of ~1 $h^+.nm^{-2}$ and a steady-state electron flux of ~25 electrons $nm^{-2}.s^{-1}$, which showed that holes were reacting approximately 25 times per second. It is this steady-state region that forms the focus of this study. When the light was turned off, holes take several seconds to react with water, and do not show the high turnover frequency observed at steady-state conditions. As we show later in the manuscript, this is most likely attributed to the requirement of multiple holes (or oxidized equivalents) to accumulate to overcome the rate limiting step of the water oxidation reaction. In the dark, there is no flux of holes to the surface, and therefore surface accumulated holes must either diffuse across the surface to accumulate and oxidize water or perhaps, as observed in previous studies of α-$Fe_2O_3$ and $BiVO_4$, perform single hole oxidations with water that are of a substantially slower reaction kinetic (TOF ~ 0.3 $s^{-1}$ in the case of $BiVO_4$).[37] The behavior of holes when the light is turned off is not studied in further detail

herein. However, coming back to the case where the light is on and a steady-state is reached, we quite strikingly observe a non-linear change in hole absorption with increasing light intensity; in contrast to the photocurrent which shows a more linear dependence with light intensity (Figure S17).

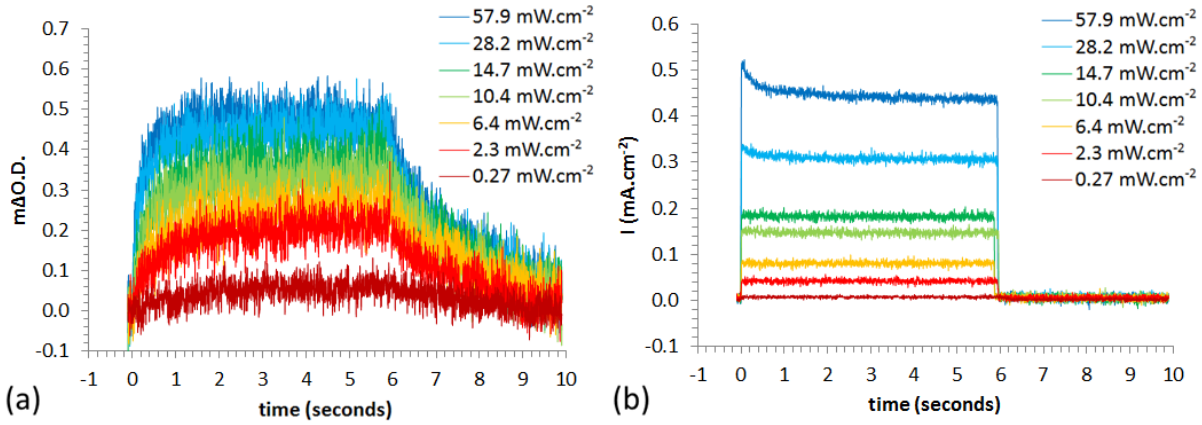


**Figure 5**. (a) Photo-induced absorption of holes at 500 nm in the anatase $TiO_2$ photoanode, measured during their oxidation of water in 1 M NaOH (pH = 13.6) at 1.5 $V_{RHE}$. The behavior was assessed at various light intensities using a continuous wave 365 nm LED light source. The LED was switched on for 6 s (0-6 s) and then off for 4 s (6 - 10 s). (b) Photocurrent transients measured simultaneously with the photo-induced absorption transients.

Our PIAS experiments were also conducted in acid (0.5 M $H_2SO_4$, pH = 0.6) and neutral (0.05 M $K_2HPO_4$ & 0.05 M $KH_2PO_4$, pH = 6.7) electrolytes. Over the wide range of pH examined, the photoelectrochemical response of the $TiO_2$ photoanode changed in line with the Nernst equation (Figure S18). In addition, the PIAS spectral features were similar, and showed that the photo-

generated states observed at 500 nm were likely the same at all pH examined (Figure S19). Moreover, with increasing light intensity, non-linear changes in the steady-state hole absorption were also observed in acid and neutral pH (Figure S20). This was once again in contrast to the photocurrent, which showed a more linear dependence with light. Over the range of light intensities examined, photocurrents ranged from ~0.5 $\mu A.cm^{-2}$ to ~0.5 $mA.cm^{-2}$, which if we consider the photocurrent such a typical $TiO_2$ photoanode would generate under one sun (by multiplying the AM 1.5 solar spectrum by the measured APCE, Figure S7), corresponds to conditions ranging from ~0.001 to ~1 sun respectively.

To analyze the difference in behavior between our optical and electrical signals, with respect to light intensity, we apply a simple kinetic model, described in detail in previous publications.[36,37] A logarithmic plot of photocurrent against the steady-state surface hole density yields a gradient of $\beta$ (the reaction order) and intercept of $k_{WO}$ (the rate constant). The absorption of holes measured by PIAS was converted into a surface hole density ($h^+.nm^{-2}$) using the hole extinction coefficient determined from TPC and TAS measurements ($\varepsilon_{h+}$ ~2000 $M^{-1}.cm^{-1}$, Figure S15).

Figure 6 shows a logarithmic plot of the surface accumulated hole density at steady-state *vs* the photocurrent density for water oxidation reaction at the three pH examined. A 2D plot is shown in Figure S21. Over the range of hole densities examined (~ 0.05 – 1 $h^+.nm^{-2}$), a third order dependence ($\beta = 2.83 \pm 0.14$, $r^2 = 0.99$) was observed in alkali (pH = 13.6). However, a second order dependence was observed in both neutral (pH = 6.7, $\beta = 2.23 \pm 0.15$, $r^2 = 0.98$) and acidic (pH = 0.6, $\beta = 2.11 \pm 0.13$, $r^2 = 0.98$) conditions. The rate constants for the water oxidation reaction were indistinguishable in neutral ($k_{WO}$ = 12 ± 1 $nm^2.s^{-1}$) and acid ($k_{WO}$ = 11 ± 1 $nm^2.s^{-1}$) pH, and changed in alkali ($k_{WO}$ = 22 ± 2 $nm^4.s^{-1}$). Apart from this change in reaction order, the rate of water oxidation was not strongly dependent on pH, with turnover frequencies (TOFs) for

hole transfer to water at ~1 sun irradiance of ~21, ~22 and ~25 $s^{-1}$ at pH's of 0.6, 6.7 and 13.6 respectively. These TOFs at 1 sun irradiance are substantially higher than those observed in $BiVO_4$ (~ 14 $s^{-1}$) and α-$Fe_2O_3$ (~ 5 $s^{-1}$),[37] where the trend tracks the valence depth in these materials (*i.e.* the oxidizing potential of holes).

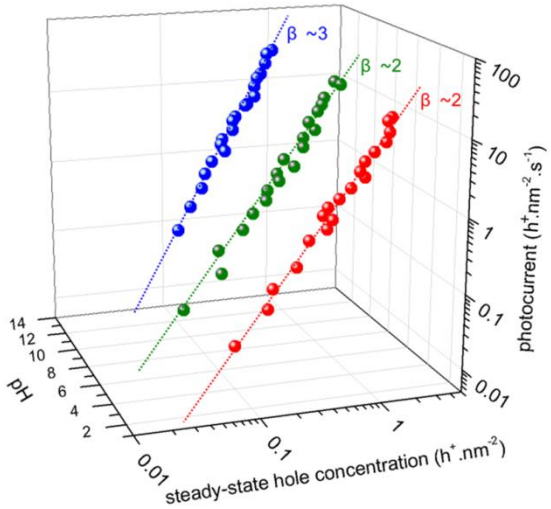


**Figure 6**. The surface hole density ($h^+.nm^{-2}$) vs photocurrent ($h^+.nm^{-2}s^{-1}$) and pH (acid, neutral or alkali) at steady-state conditions during the oxidation of water by $TiO_2$ (1.5 $V_{RHE}$) at various LED light intensities (~0.1 – 60 $mW.cm^{-2}$). The electrolytes used were 1 M NaOH (pH = 13.6), 0.05 M $K_2HPO_4$ & 0.05 M $KH_2PO_4$ (pH = 6.7) and 0.5 M $H_2SO_4$ (pH = 0.6). In acid and neutral media, the lines of best fit show a second order dependence, with respect to the hole density, and in alkali, a third order dependence.

## 4. POSSIBLE WATER OXIDATION MECHANISMS ON TITANIA

Our PIAS studies shows that at conditions similar to practical device operation a concerted oxidation of water occurs on $TiO_2$, as the rate limiting step requires the accumulation of two or more holes. In acidic and neutral conditions, a second order reaction was observed, with respect to the hole density. In alkaline conditions, a third order reaction was observed.

The reaction order and kinetics of water oxidation was previously studied by Le Formal *et. al.* on α-$Fe_2O_3$ photoanodes in alkali (1 M NaOH, pH 13.6).[36] Similar to this study, a third order reaction was also observed (above a surface hole density threshold). Ma *et. al.* also studied the water oxidation reaction on $BiVO_4$ photoanodes in neutral conditions (phosphate buffer, pH 6.7).[37] A third order dependence was also observed. Nonetheless, there were two key differences in the behaviors of α-$Fe_2O_3$ and $BiVO_4$ compared with $TiO_2$. Firstly, the rate constants were considerably lower in α-$Fe_2O_3$ ($k_{WO}$ = 0.5 $nm^4.s^{-1}$) and $BiVO_4$ ($k_{WO}$ = 0.8 $nm^4.s^{-1}$) compared to the $TiO_2$ studied herein ($k_{WO}$ ~22 $nm^4.s^{-1}$), which we attribute to the less positive, and thus less oxidizing valence band energies present in these materials.[55] Secondly, in both α-$Fe_2O_3$ and $BiVO_4$ a transition to a first order reaction was observed at low hole densities (below ~1 $h^+.nm^{-2}$ in both α-$Fe_2O_3$ and $BiVO_4$). In this study of $TiO_2$, a first order reaction was not observed over the range of hole densities examined (~ 0.05 – 1 $h^+.nm^{-2}$). This transition from a first to third order reaction on α-$Fe_2O_3$ was previously attributed to the static nature of surface holes on this material, and the requirement for holes to be present on neighboring sites for a concerted reaction to occur.[36] We therefore tentatively attribute the lack of a first order reaction order on $TiO_2$ to a higher mobility of surface holes, where previous studies have shown that surface holes (or their oxidized equivalent) on $TiO_2$ are highly mobile and can migrate for several microns before reacting.[56]

Now we turn to analyze the water oxidation reaction mechanism on $TiO_2$ at different pH. From the experiments above we can extract three main ideas: (i) the rate limiting step (RLS) of the catalytic cycle changes with pH, with three accumulated holes required in alkaline pH, and two accumulated holes required in neutral and acidic pH to overcome the RLS, which denotes a change of mechanism at high pH; (ii) the Nernstian dependency of the RLS, in which we observe

a similar onset of photocatalysis when represented on a RHE scale (Figure S18). Finally, a hydroxyl nucleophilic attack is most probably not included in the RLS, since the rate of water oxidation is similar over the wide range of pH studied herein.

In the literature there are several publications dealing with the understanding of this mechanism. The first step of the cycle consists in the photo-generation of a surface hole. However its specific location is debated in the literature: some place it on a terminal hydroxyl group Ti-OH[24,25]; however, others argue that it generates on surface Ti-O-Ti bridging sites.[26–30] Evidence for $\dot{O}H$ formation has been provided from diffuse reflectance FT-IR spectroscopy,[34] scanning tunneling microscopy[57] and by using spin trapping agents during electron paramagnetic resonance (EPR) spectroscopy.[31–33] The formation of these type of photo-generated holes is further detected by DFT calculations.[58,59]

The water oxidation mechanism is well studied and better understood in molecular catalysts. The most accepted reaction pathways involve water nucleophilic attack and the formation of an M-O-O-M bond. This implies that small changes in the systems such as orientation of the active groups, or pH, will drive a change in reaction mechanism.[60]

The formation of Ti-O-O-Ti groups have previously been observed in the literature. Time-resolved diffuse reflectance FT-IR studies have detected the presence of surface peroxo and oxyhydroxo bonds on $TiO_2$.[39] This is not exclusive to $TiO_2$, with oxy-hydroxide bond formation also observed on $Co_3O_4$ during electrocatalytic water oxidation.[38] Thus, by a proton-coupled electron transfer (PCET) reaction,[61] it is possible that a second hole can react, when adjacent to a chemically bound hydroxyl radical ȮH, and form a surface peroxo Ti-O-O-Ti bond.[39] This reaction pathway would agree with the second order dependency found at neutral and acidic pH.

On the other hand at high pH, three accumulated holes are needed to overcome the RLS of the catalytic cycle. The same dependency has previously been found on α-$Fe_2O_3$ at pH ~14[32] and $BiVO_4$ at pH ~7.[33] These studies showed that three surface holes interact in the RLS, and may be associated with oxy-hydroxide formation during the water oxidation reaction. Previous observation of surface oxy-hydroxide formation have not always been associated with the initial formation of an M-O-O-M bond.[38] For example in the case of $Co_3O_4$ case, surface oxy-hydroxide species are formed after nucleophilic attack by water with a surface hole on a Co=O oxo site. A similar mechanism has been proposed from DFT studies of GaN.[62] This would indicate that similar species could also drive water oxidation through water nucleophilic attack.

The exact nature of what drives the change in reaction mechanism in $TiO_2$ is beyond the scope of this paper. Some DFT studies have showed that the first PCET is sequential, with electron transfer following proton transfer, and at high pH was barrierless, where the rate was determined by the concentration of surface $OH^-$.[63] However, to our knowledge, the energetics of successive oxidations of water on $TiO_2$ have not been calculated. However, this study shows that a change in $OH^-$ concentration induces changes in the $TiO_2$ surface, which changes the energetics of the surfaces holes and the mechanism by which water is oxidized. This change may be associated with surface deprotonation, as third order behavior is commonly observed in α-$Fe_2O_3$ (PZC ~9),[32] $BiVO_4$ (PZC ~3)[33] and $TiO_2$ (PZC ~6-7) herein above their point of zero charge (PZC).

Although the wide bandgap of $TiO_2$ severely limits solar activity, ultra-thin coatings are widely used to protect narrow bandgap semiconductors susceptible to photocorrosion (e.g. Si[64] and $Cu_2O$[11]) and inhibit surface recombination (e.g. α-$Fe_2O_3$[65] and $BiVO_4$[66]) in a range of photoanode materials. Therefore, increasing our understanding of the catalytic properties of $TiO_2$ remains an important topic. Moreover, $TiO_2$ is a versatile photocatalyst, and can decompose a wide range of

organic media (*e.g.* bacteria, NOx gas *etc*) and is applied commercially in self-cleaning windows and tiles.[67] As such, this study opens the door to the rate law analyses of a number of commercially relevant processes.

## CONCLUSION

The water oxidation reaction on anatase $TiO_2$ photoanodes was investigated using complementary spectroscopic techniques to provide new insight into the reaction mechanism. Transient absorption spectroscopy (TAS) studies showed that water oxidation by surface holes was the kinetically limiting process, where the kinetics of water oxidation by photo-generated holes on $TiO_2$ ($t_{50\%}$ ~100 ms) was nearly three orders of magnitude slower than electron extraction ($t_{50\%}$ ~200 μs).

Under conditions similar to device operation (from ~0.001 – 1 sun), the behavior of photo-generated holes was assessed using photo-induced absorption spectroscopy (PIAS). The surface hole density increased non-linearly with photocurrent, irrespective of pH. Using an appropriate kinetic model, the reaction order with respect to holes was deduced. In alkaline conditions, a third order reaction was observed, similar to previous studies of α-$Fe_2O_3$ and $BiVO_4$. In this regime, the rate constant for water oxidation was substantially greater on $TiO_2$ ($k_{WO}$ ~22 $nm^4.s^{-1}$) compared with α-$Fe_2O_3$ ($k_{WO}$ = 0.5 $nm^4.s^{-1}$) and $BiVO_4$ ($k_{WO}$ = 0.8 $nm^4.s^{-1}$), which we attribute to the more positive, and thus more oxidizing valence band of $TiO_2$. In acidic and neutral conditions, a second order reaction was observed on $TiO_2$. This showed that the observable rate limiting step required holes (or their oxidized equivalents) to accumulate for water oxidation to take place, and that the number of holes (or their oxidized equivalents) that accumulate changes with pH. This change might be associated with surface deprotonation, as third order behavior

was observed on $TiO_2$ herein, and previously in $\alpha$-$Fe_2O_3$ and $BiVO_4$, above their point of zero charge.

For two or more surface holes to take part in the RLS of the water oxidation reaction, it is likely that the mechanism involves PCET steps. This behavior is consistent with recent observations of peroxo and hydroperoxo intermediates formed on $TiO_2$, and other metal oxide surfaces, during water oxidation. Importantly, at conditions similar to device operation, the change in reaction order did not impact substantially on the reaction rate, which corresponded to a TOF per surface hole in the region of 20 – 25 $s^{-1}$ at conditions similar to 1 sun irradiance. This shows that the RLS does not involve $OH^-$ nucleophilic attack, otherwise more substantial changes in reaction rate would have been observed with such drastic changes in pH. As little variation in reaction rate (*i.e.* hole TOF) was observed, these studies demonstrate the versatility of $TiO_2$ as an active water oxidation photocatalyst over a wide range of pH.

## ACKNOWLEDGMENTS

JRD thanks the European Research Council (project Intersolar 291482) for funding. AK thanks Imperial College for a Junior Research Fellowship. L.F. thanks the CEC for the award of a Marie Curie Fellowship. CJC wishes to thank the EPSRC for funding (EP/K001515).

## SUPPORTING INFORMATION

Details of synthesis, physical and functional characterization; XRD and Raman analysis; AFM images; HRTEM lattice spacing; UV-visible absorption spectroscopy; Swanepoel film thickness measurements; Mott-Schottky plot; APCE measurements and optical penetration depth; additional TPC and TAS data; calculation of the extinction coefficient of a hole in $TiO_2$; additional PIAS data measured in acidic, neutral and alkaline conditions.

**Funding Sources**

European Research Council (project Intersolar 291482), EPSRC for funding (EP/K001515).

## ABBREVIATIONS

APCE, absorbed photon to current efficiency; APCVD, atmospheric pressure chemical vapor deposition; AFM, atomic force microscopy; HRTEM, high resolution transmission electron microscopy; SEM, scanning electron microscopy; PIAS, photo-induced absorption spectroscopy; TAS, transient absorption spectroscopy; TPC, transient photocurrent; $V_{RHE}$, applied potential *vs* the reversible hydrogen electrode; XPS, X-ray photoelectron spectroscopy; XRD, X-ray diffraction.

## REFERENCES

(1) Fujishima, A.; Honda, K. *Nature* **1972**, *238*, 37–38.

(2) Mills, A.; Le Hunte, S. *J. Photochem. Photobiol. A Chem.* **1997**, *108*, 1–35.

(3) Zhang, H.; Chen, G.; Bahnemann, D. W. *J. Mater. Chem.* **2009**, *19*, 5089–5121.

(4) Chen, Y.; Hu, S.; Xiang, C.; Lewis, N. S. *Energy Environ. Sci.* **2015**, *8*, 876–886.

(5) Kafizas, A.; Parkin, I. P. *J. Mater. Chem.* **2010**, *20*, 2157–2169.

(6) Kafizas, A.; Crick, C. R.; Parkin, I. P. *J. Photochem. Photobiol. A Chem.* **2010**, *216*, 156–166.

(7) Dunnill, C. W.; Aiken, Z. A.; Kafizas, A.; Pratten, J.; Wilson, M.; Morgan, D. J.; Parkin,

I. P. *J. Mater. Chem.* **2009**, *19*, 8747–8754.

(8) Kafizas, A.; Noor, N.; Carmichael, P.; Scanlon, D. O.; Carmalt, C. J.; Parkin, I. P. *Adv. Funct. Mater.* **2014**, *24*, 1758–1771.

(9) Kafizas, A.; Kellici, S.; Darr, J. A.; Parkin, I. P. *J. Photochem. Photobiol. A Chem.* **2009**, *204*, 183–190.

(10) Kafizas, A.; Dunnill, C. W.; Parkin, I. P. *J. Mater. Chem.* **2010**, *20*, 8336–8349.

(11) Paracchino, A.; Laporte, V.; Sivula, K.; Grätzel, M.; Thimsen, E. *Nat. Mater.* **2011**, *10*, 456–461.

(12) Sotelo-Vazquez, C.; Quesada-Cabrera, R.; Ling, M.; Scanlon, D. O.; Kafizas, A.; Thakur, P. K.; Lee, T.-L.; Taylor, A.; Watson, G. W.; Palgrave, R. G.; Durrant, J. R.; Blackman, C. S.; Parkin, I. P. *Adv. Funct. Mater.* **2017**, 1605413.

(13) Ferreira, K. N.; Iverson, T. M.; Maghlaoui, K.; Barber, J.; Iwata, S. *Science.* **2004**, *303*, 1831–1838.

(14) Sala, X.; Romero, I.; Rodriguez, M.; Escriche, L.; Llobet, A. *Angew. Chemie* **2009**, *48*, 2842–2852.

(15) Najafpour, M. M.; Ehrenberg, T.; Wiechen, M.; Kurz, P. *Angew. Chemie* **2010**, *49*, 2233–2237.

(16) Osterloh, F. E. *Chem. Soc. Rev.* **2013**, *42*, 2294–2320.

(17) Grätzel, M. *Nature* **2001**, *414*, 338–344.

(18) Cowan, A. J.; Durrant, J. R. *Chem. Soc. Rev.* **2013**, *42*, 2281–2293.

(19) Kim, T. W.; Choi, K.-S. *Science.* **2014**, *343*, 990–994.

(20) Kanan, M. W.; Nocera, D. G. *Science.* **2008**, *321*, 1072–1075.

(21) Lin, F.; Boettcher, S. W. *Nat. Mater.* **2013**, *13*, 81–86.

(22) Dau, H.; Limberg, C.; Reier, T.; Risch, M.; Roggan, S.; Strasser, P. *ChemCatChem* **2010**, *2*, 724–761.

(23) Nakato, Y.; Ogawa, H.; Moria, K.; Tsubomura, H. *J. Phys. Chem.* **1986**, *90*, 6210–6216.

(24) Wilson, R. H. *J. Electrochem. Soc.* **1980**, *127*, 228–234.

(25) Zigah, D.; Rodríguez-López, J.; Bard, A. J. *Phys. Chem. Chem. Phys.* **2012**, *14*, 12764–12772.

(26) Howe, R. F.; Graetzel, M. *J. Phys. Chem.* **1987**, *91*, 3906–3909.

(27) Micic, O. I.; Zhang, Y.; Cromack, K. R.; Trifunac, A. D.; Thurnauer, M. C. *J. Phys. Chem.* **1993**, *97*, 7277–7283.

(28) Micic, O. I.; Zhang, Y.; Cromack, K. R.; Trifunac, A. D.; Thurnauer, M. C. *J. Phys. Chem.* **1993**, *97*, 13284–13288.

(29) Kisumi, T.; Tsujiko, A.; Murakoshi, K.; Nakato, Y. *J. Electroanal. Chem.* **2003**, *545*, 99–107.

(30) Tsujiko, A.; Kisumi, T.; Magari, Y.; Murakoshi, K.; Nakato, Y. *J. Phys. Chem. B* **2000**,

*104*, 4873–4879.

(31) Grela, M. A.; Coronel, M. E. J.; Colussi, A. J. *J. Phys. Chem.* **1996**, *100*, 16940–16946.

(32) Jaeger, C. D.; Bard, A. J. *J. Phys. Chem.* **1979**, *83*, 3146–3152.

(33) Riegel, G.; Bolton, J. R. *J. Phys. Chem.* **1995**, *99*, 4215–4224.

(34) Szczepankiewicz, S. H.; A. Colussi, J.; Hoffmann, M. R. *J. Phys. Chem. B* **2000**, *104*, 9842–9850.

(35) Li, R.; Weng, Y.; Zhou, X.; Wang, X.; Mi, Y.; Chong, R.; Han, H.; Li, C. *Energy Environ. Sci.* **2015**, *8*, 2377–2382.

(36) Le Formal, F.; Pastor, E.; Tilley, S. D.; Mesa, C. A.; Pendlebury, S. R.; Grätzel, M.; Durrant, J. R. *J. Am. Chem. Soc.* **2015**, *137*, 6629–6637.

(37) Ma, Y.; Mesa, C. A.; Pastor, E.; Kafizas, A.; Francàs, L.; Le Formal, F.; Pendlebury, S. R.; Durrant, J. R. *ACS Energy Lett.* **2016**, *1*, 618–623.

(38) Zhang, M.; Respinis, M. De; Frei, H. *Nat. Chem.* **2014**, *6*, 362–367.

(39) Nakamura, R.; Nakato, Y. *J. Am. Chem. Soc.* **2004**, *126*, 1290–1298.

(40) Burdett, J. K.; Hughbanks, T.; Miller, G. J.; Richardson, J. W.; Smith, J. V. *J. Am. Chem. Soc.* **1987**, *109*, 3639–3646.

(41) Tauc, J. *Mater. Res. Bull.* **1968**, *3*, 37–46.

(42) Swanepoel, R. J. *J. Phys. E.* **1983**, *16*, 1214–1222.

(43) Boschloo, G. K.; Goossens, A.; Schoonman, J. *J. Electrochem. Soc.* **1997**, *144*, 1311–1317.

(44) Formal, F. Le; Pendlebury, S. R.; Cornuz, M.; Tilley, S. D.; Graetzel, M.; Durrant, J. R. *J. Am. Chem. Soc.* **2014**, *136*, 2564–2574.

(45) Ma, Y.; Pendlebury, S. R.; Reynal, A.; Le Formal, F.; Durrant, J. R. *Chem. Sci.* **2014**, *5*, 2964–2973.

(46) Peter, L. M.; Wijayantha, K. G. U.; Tahir, A. A. *Faraday Discuss.* **2012**, *155*, 309–322.

(47) Kafizas, A.; Wang, X.; Pendlebury, S. R.; Barnes, P. R. F.; Ling, M.; Sotelo-Vazquez, C.; Quesada-Cabrera, R.; Li, C.; Parkin, I. P.; Durrant, J. R. *J. Phys. Chem. A* **2016**, *120*, 715–723.

(48) Wang, X.; Kafizas, A.; Li, X.; Moniz, S. J. A.; Reardon, P. J. T.; Tang, J.; Parkin, I. P.; Durrant, J. R. *J. Phys. Chem. C* **2015**, *119*, 10439–10447.

(49) Cowan, A. J.; Leng, W.; Barnes, P. R. F.; Klug, D. R.; Durrant, J. R. *Phys. Chem. Chem. Phys.* **2013**, *15*, 8772.

(50) Cowan, A. J.; Leng, W.; Barnes, P. R. F.; Klug, D. R.; Durrant, J. R. *PCCP* **2013**, *15*, 8772–8778.

(51) Pesci, F. M.; Wang, G.; Klug, D. R.; Li, Y.; Cowan, A. J. *J. Phys. Chem. C* **2013**, *117*, 25837–25844.

(52) Barroso, M.; Mesa, C. A.; Pendlebury, S. R.; Cowan, A. J.; Hisatomi, T.; Sivula, K.; Grätzel, M.; Klug, D. R.; Durrant, J. R. *Proc. Natl. Acad. Sci.* **2012**, *109*, 15640–15645.

(53) Cowan, A. J.; Tang, J.; Leng, W.; Durrant, J. R.; Klug, D. R. *J. Phys. Chem. C* **2010**, *114*, 4208–4214.

(54) Pendlebury, S. R.; Wang, X.; Le Formal, F.; Cornuz, M.; Kafizas, A.; Tilley, S. D.; Grätzel, M.; Durrant, J. R. *J. Am. Chem. Soc.* **2014**, *136*, 9854–9857.

(55) Chen, S.; Wang, L.-W. *Chem. Mater.* **2012**, *24*, 3659–3666.

(56) Haick, H.; Paz, Y. *Chemphyschem* **2003**, *4*, 617–620.

(57) Tan, S.; Feng, H.; Ji, Y.; Wang, Y.; Zhao, J.; Zhao, A.; Wang, B.; Luo, Y.; Yang, J.; Hou, J. G. *J. Am. Chem. Soc.* **2012**, *2*, 9978–9985.

(58) Ji, Y.; Wang, B.; Luo, Y. *J. Phys. Chem. C* **2014**, *2*, 1027–1034.

(59) Cheng, J.; Vandevondele, J.; Sprik, M. *J. Phys. Chem. C* **2014**, *118*, 5437–5444.

(60) Blakemore, J. D.; Crabtree, R. H.; Brudvig, G. W. *Chem. Rev.* **2015**, *115*, 12974–13005.

(61) Schrauben, J. N.; Hayoun, R.; Valdez, C. N.; Braten, M.; Fridley, L.; Mayer, J. M. *Science.* **2012**, *336*, 1298–1301.

(62) Ertem, M. Z.; Kharche, N.; Batista, V. S.; Hybertsen, M. S.; Tully, J. C.; Muckerman, J. T. *ACS Catal.* **2015**, *5*, 2317–2323.

(63) Chen, J.; Li, Y.; Sit, P.; Selloni, A. *J. Am. Chem. Soc.* **2013**, *135*, 18774–18777.

(64) Hu, S.; Shaner, M. R.; Beardslee, J. A.; Lichterman, M.; Brunschwig, B. S.; Lewis, N. S. *Science.* **2014**, *344*, 1005–1009.

(65) Ahmed, M. G.; Kretschmer, I. E.; Kandiel, T. A.; Ahmed, A. Y.; Rashwan, F. A.; Bahnemann, D. W. *ACS Appl. Mater. Interfaces* **2015**, *7*, 24053–24062.

(66) Zhang, Y.; Zhang, X.; Wang, D.; Wan, F.; Liu, Y. *Appl. Surf. Sci.* **2017**, *403*, 389–395.

(67) Fujishima, A.; Zhang, X.; Tryk, D. *Surf. Sci. Rep.* **2008**, *63*, 515–582.